RESEARCH ARTICLE | DECEMBER 15 2023

# Synaptic plasticity emulation by natural biomaterial honey-CNT-based memristors **⑤ ⑥ ⊘**

Zoe Templin (□); Md Mehedi Hasan Tanim (□); Feng Zhao 🗷 (□)

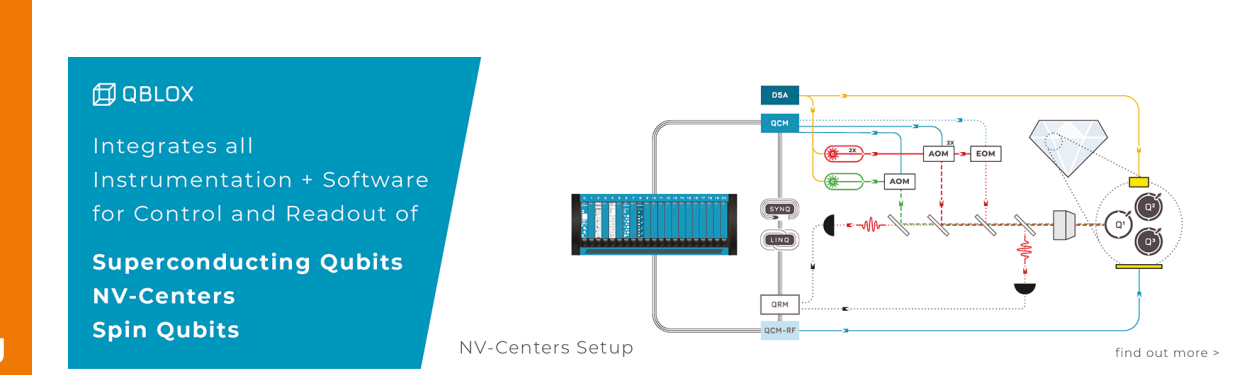


Appl. Phys. Lett. 123, 243301 (2023) https://doi.org/10.1063/5.0174426





CrossMark





### Synaptic plasticity emulation by natural biomaterial honey-CNT-based memristors (1) (3)

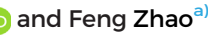
Cite as: Appl. Phys. Lett. 123, 243301 (2023); doi: 10.1063/5.0174426 Submitted: 31 August 2023 · Accepted: 4 November 2023 · Published Online: 15 December 2023







Zoe Templin, 🕞 Md Mehedi Hasan Tanim, 🕞 and Feng Zhao 🖰 🕞





### **AFFILIATIONS**

Micro/Nanoelectronic and Energy Laboratory, School of Engineering and Computer Science, Washington State University, Vancouver, Washington 98686, USA

<sup>a)</sup>Author to whom correspondence should be addressed: feng.zhao@wsu.edu

### **ABSTRACT**

Artificial synaptic devices made from natural biomaterials capable of emulating functions of biological synapses, such as synaptic plasticity and memory functions, are desirable for the construction of brain-inspired neuromorphic computing systems. The metal/dielectric/metal device structure is analogous to the pre-synapse/synaptic cleft/post-synapse structure of the biological neuron, while using natural biomaterials promotes ecologically friendly, sustainable, renewable, and low-cost electronic devices. In this work, artificial synaptic devices made from honey mixed with carbon nanotubes, honey-carbon nanotube (CNT) memristors, were investigated. The devices emulated spike-timingdependent plasticity, with synaptic weight as high as 500%, and demonstrated a paired-pulse facilitation gain of 800%, which is the largest value ever reported. 206-level long-term potentiation (LTP) and long-term depression (LTD) were demonstrated. A conduction model was applied to explain the filament formation and dissolution in the honey-CNT film, and compared to the LTP/LTD mechanism in biological synapses. In addition, the short-term and long-term memory behaviors were clearly demonstrated by an array of  $5 \times 5$  devices. This study shows that the honey-CNT memristor is a promising artificial synaptic device technology for applications in sustainable neuromorphic computing.

Published under an exclusive license by AIP Publishing. https://doi.org/10.1063/5.0174426

Despite the many undeniable benefits of current computer technology, the bottleneck of current von Neumann architecture results in a massive consumption of power and energy. In addition, the obsolescence of aging hardware components produces electronic waste that continues to grow every year and harm the environment.<sup>2,3</sup> As a potential solution, brain-inspired neuromorphic computing has attracted research attention for reducing computational power consumption.<sup>4,5</sup> To develop such computing systems, device technologies that can emulate the functions of basic building blocks of the brain, or synapses, is needed. Memristors are a potential technology being developed for such artificial synaptic devices.

Natural biomaterials, such as proteins and sugars, have attracted interest as the dielectric layer of memristors for nonvolatile memory and artificial synaptic devices due to their environmentally friendly nature while also being biodegradable and sustainable, 6-12 posing a potential solution to reduce electronic waste. Among these biomaterials, honey, a mixture of mono-, di-, and polysaccharides, is a natural preservative and is abundant, sustainable, and dissolvable. Honey has been demonstrated as a viable dielectric in memristors for its nonvolatile attributes 13,14 and ability to effectively emulate synaptic properties. 15-18 When incorporating carbon nanotubes (CNTs) in honey, a honey-CNT artificial synaptic device has been found to enhance the nonvolatile memory behaviors including voltage set/reset and retention, <sup>19</sup> and synaptic plasticity emulation. <sup>20</sup> In this work, honey-CNT synaptic devices were fabricated and evaluated to emulate synaptic plasticity, including spike-timing-dependent plasticity (STDP), pairedpulse facilitation (PPF), long-term potentiation (LTP), and long-term depression (LTD). A conduction model was established and compared to the LTP/LTD mechanism in biological synapses. STM and LTM are demonstrated by a  $5 \times 5$  device array. These test results indicate that honey-CNT memristors are promising for making artificial synaptic devices in energy efficient and environmentally friendly neuromorphic computing systems.

The honey-CNT solution was prepared by mixing commercial honey and de-ionized water for a 30% concentration by weight. Singlewall CNT powders, as-received (P0286 HiPco SWCNTs, Carbon Nanotechnologies Inc.), were dispersed into the honey solution for a 0.2% wt concentration in a 60 min ultrasonic bath. This formed the honey-CNT solution. The solution was then placed in vacuum for 24 h until the honey was fully dissolved, and all air bubbles in the solution were removed. The glass substrate  $(2.5 \times 2.5 \text{ cm}^2)$  was cleaned in an ultrasonic bath of acetone, isopropyl alcohol (IPA), then de-ionized

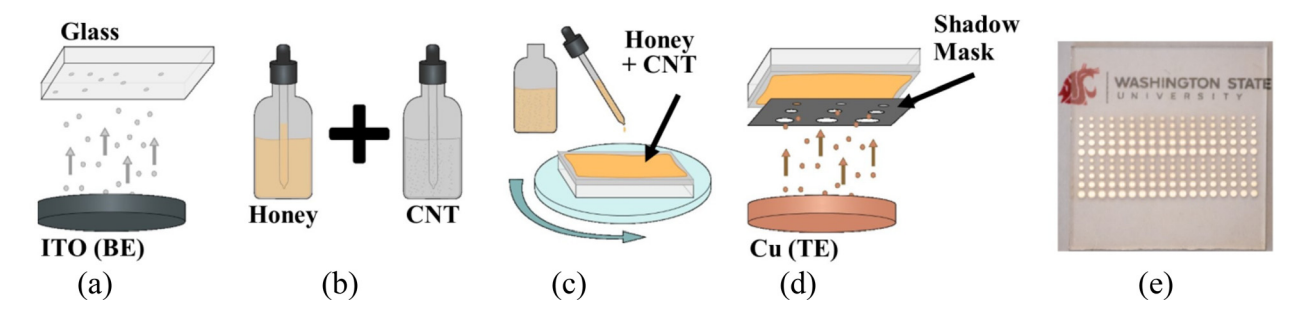


FIG. 1. Schematic fabrication process flow of honey-CNT memristors: (a) deposition of ITO bottom electrode onto a glass substrate, (b) mixing honey and CNT solution, (c) spin coating of honey-CNT solution on the ITO electrode, followed by baking, (d) deposition of Cu top electrodes through a shadow mask, and (e) final devices after fabrication.

water for 10 min each, and dried by  $N_2$  gas. ITO (10  $\Omega$ /sq) deposition onto the glass substrate was carried out in a Kurt J. Lesker Nano 36 DC/RF sputter system to form the bottom electrode. This was followed by spin coating of the honey-CNT solution at 3000 rpm for 90 s. The sample was then baked in an oven for 6 h at 120 °C to dry the honey-CNT thin film. Finally, the Cu top electrodes were deposited via sputtering through a stencil mask with circular openings. The circular openings included diameters of 100, 200, 300, 400, and 500  $\mu$ m. A schematic diagram of the fabrication process and a photograph of the sample are shown in Fig. 1.

All electrical testing was conducted on a semi-automatic probe station (Signatone S1160B) at room temperature in air. A Siglent SDG 1032X function arbitrary waveform generator and a Rigol MSO5204 digital oscilloscope were used to apply input voltage pulses and record output voltage responses. A  $20\,k\Omega$  resistor was placed in series with the honey-CNT memristor output to the oscilloscope for calculating the current output of the device.

Demonstration of potentiation and depression is important for showing the potential of an artificial synaptic device to emulate the synaptic plasticity that occurs in biological synapses. Potentiation and depression in biological synapses are behaviors that strengthen and weaken the synaptic weight. In this test, the action potentials were mimicked by a voltage pulse train. A total of 412 consecutive voltage pulses of equal amplitude and pulse width (0.9 V, 10 ms) were applied on the honey-CNT memristor. The first 206 pulses were positively biased, followed by 206 negatively biased pulses. The output current represents the synaptic weight. The normalized current in Fig. 2 shows that the synaptic strength gradually increases (synaptic potentiation) during the application of positive pulses and then decreases (synaptic depression) when negative pulses are implemented. The results are comparable to other artificial synaptic devices made from natural biomaterials such as collagen,8 which showed potentiation and depression by a train of 400 voltage pulses.

The principal mechanisms for the synaptic behaviors of a honey-CNT memristor can be attributed to the electrochemical redox of the Cu top electrode for the formation and dissolution of conductive filaments in the honey-CNT film. Figure 3 depicts an analogy between this electrochemical redox mechanism of the honey-CNT memristor and the biochemical mechanism of biological synapses for LTP and LTD. Figure 3(a) shows the stationary CNT bundles and clusters in the pristine honey-CNT film. When positive voltage pulses are initially applied on the Cu top electrode, Cu atoms are oxidized to positive Cu ions, which, under the electric field, drift downward the ITO bottom

electrode and reduce to Cu atoms by free electrons from the ITO electrode, as shown in Fig. 3(b). Cu atoms accumulate on the bottom electrode and eventually reach the top electrode, forming conductive paths (filaments), as shown in Fig. 3(c). During the filament formation, CNT clusters and bundles remain stationary within the honey-CNT film, but due to their ability to increase electrical conductivity, specifically via charge carriers, 21-23 they assist with the formation of stable filaments to improve synaptic behaviors. Continuing to apply positive voltage pulses results in more filament pathways [Fig. 3(d)], increasing the flow of electrons in the honey-CNT film and, therefore, the current, as in the LTP shown by Fig. 2. This is similar to the biochemical mechanism of a biological synapse during LTP, as shown in Figs. 3(e) and 3(f), which also exhibits physical changes within the synapse itself.<sup>24</sup> During LTP, the presynaptic vesicles see an increase in neurotransmitters, and the number of neurotransmitter receptors increase in the post-synapse, leading to higher excitatory postsynaptic current (EPSC) in the synapse—synaptic potentiation. 24-26 When compared to a honey-CNT memristor, an applied voltage pulse on the Cu top electrode is analogous to an action potential on the pre-synapse, the Cu ions resemble the neurotransmitters in the synaptic cleft, the conductive filaments resemble the neurotransmitter receptors, and the current flow through the device is analogous to the EPSC of the biological synapse. When continuous negative voltage pulses are applied

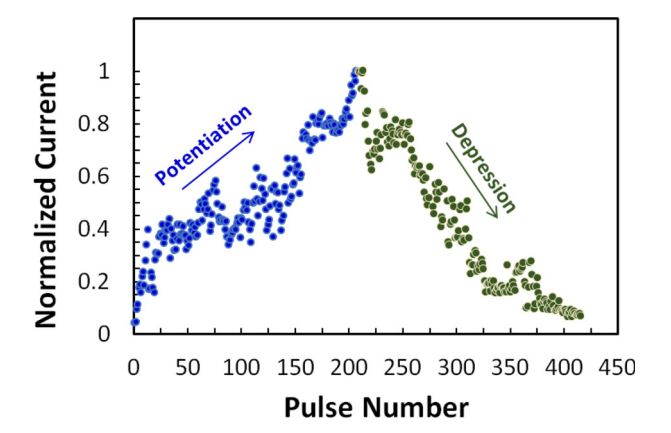


**FIG. 2.** Current response showing potentiation (blue dots) and depression (green dots) when a train of 412 V pulses including 206 positive followed by 206 negative pulses were applied on the honey-CNT memristor. The amplitude and width of the pulses were 0.9 V and 10 ms, respectively.

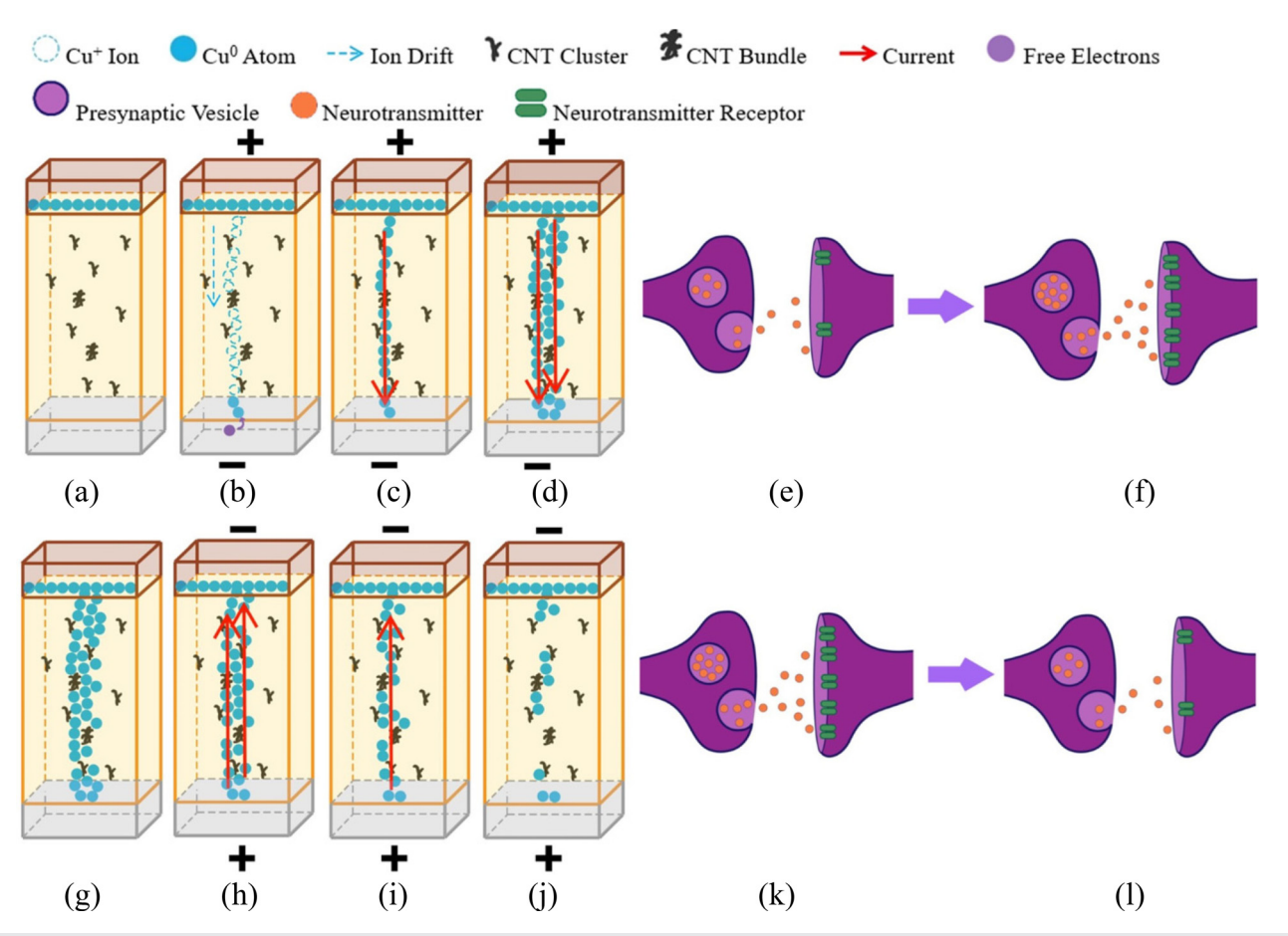


FIG. 3. Analogy of conductive path formation and dissolution in honey-CNT memristor to a biological neuron for LTP and LTD: (a) pristine device, (b)–(d) continuous positive voltage pulses are applied on the honey-CNT memristor, (e)–(f) continuous action potentials are applied to a biological synapse due to high synapse activity, (g) device is potentiated, and applied voltage pulses are removed, and the device retains the conductive paths, (h)–(j) continuous negative voltage pulses are applied for a long time until conductive paths are dissolved by joule heating, and (k)–(l) when fewer or no continuous action potentials are applied to the biological synapse due to lower synapse activity.

following the positive voltage pulses, the Cu filaments gradually dissolve due to joule heating [Figs. 3(h) and 3(i)], resulting in a decrease in the conductance within the device and, therefore, the current, as shown in the LTD by Fig. 2. Eventually, all conductive paths are dissolved, and the current in the device returns to zero [Fig. 3(j)]. The mechanism of the LTD is also similar to that occurring in a biological synapse, and the physical changes of the synapse during the LTD lead to a decrease in neurotransmitters (Cu ions) and neurotransmitter receptors (conductive filaments) [Figs. 3(k) and 3(l)].

PPF was used to demonstrate the capability of the artificial synaptic device's short-term plasticity. In this test, two consecutive pulses (1.2 V amplitude and 100 ms width) with time intervals  $\Delta t$  ranging between 20 and 2000 ms were applied to mimic the presynaptic spikes of biological neurons. Figure 4(a) shows the current responses of A<sub>1</sub> and A<sub>2</sub>, which are synonymous to the EPSC response of the post-synapse. The PPF index, defined as the ratio of the absolute amplitude of the output currents A<sub>1</sub>/A<sub>2</sub>, is used to quantify the PPF effect. Shown in Fig. 4(b), a gain of 800% is achieved at a  $\Delta t$  of 20 ms, which is higher than a previously reported honey-memristor 14,17 and comparable with

other natural biomaterials.<sup>29,30</sup> Much like in biological synapses, there are factors that increase the probability of neurotransmitter release and influence the PPF gain and short-term plasticity.<sup>28,31</sup> For honey-CNT memristors, the high gain is likely attributed to CNTs that facilitate the growth of conductive filaments, similar to increasing the probability of neurotransmitter release.

It is also observed in Fig. 4(b) that as  $\Delta t$  increases, A1/A2 decreases. This holds true to how biological synapses behave. The PPF index of biological synapses can be modeled with a double exponential decay with one rapid phase and the other slow phase  $^{32,33}$  as

$$PPF = c_1 e^{-\frac{\Delta t}{\tau_1}} + c_2 e^{-\frac{\Delta t}{\tau_2}} + 1, \tag{1}$$

where  $c_1$  and  $c_2$  represent the initial magnitudes of the presynaptic spikes and  $\tau_1$  and  $\tau_2$  correspond to the characteristic relaxation times of the rapid and slow phases. As shown in Fig. 4(b), the fitted curve using Eq. (1) agrees well with the experimental data. The fast phase  $(c_1 = 200\%, \ \tau_1 = 17 \ \text{ms})$  and slow phase  $(c_2 = 700\%, \ \tau_2 = 390 \ \text{ms})$  of the honey-CNT synaptic memristor are comparable to typical biological synapses.

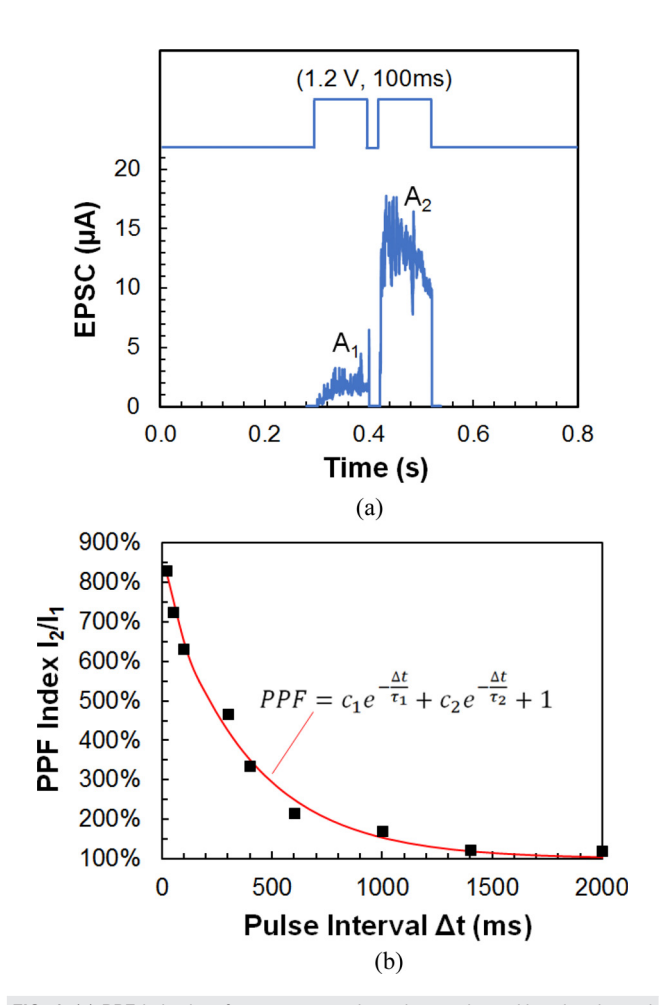


**FIG. 4.** (a) PPF behavior after two consecutive voltage pulses with a time interval  $\Delta t$  of 20 ms were applied. (b) PPF index as a function of  $\Delta t$ . Black squares: experimental data, red curve: the double-exponential model fit.

Long-term memory (LTM) and short-term memory (STM) are essential functions of the human brain. They are differentiable by the firing rate and number of action potentials at the pre-synapse, as memory depends greatly on brain activity at any given moment. 34,35 STM and LTM functions were explored on honey-CNT memristors by mimicking the concurrent action potentials on a pre-synapse by voltage pulse stimuli, with resulted currents (EPSC) from the device distinguishing between STM and LTM. A 5 × 5 memristor array was used in this test, with each device representing a pixel. These 25 pixels were used to memorize two letters, "E" and "X." The array memorized the letter "E" using the STM stimuli, and the letter "X" by the LTM stimuli at the same time. These stimuli are shown in Fig. 5(a) with their corresponding letter layout on the devices, and form combined stimuli when the letters overlap. The STM "E" stimuli consist of a train of 10 voltage pulses (1.4 V, 10 ms) at a lower frequency of 5 Hz in order to form weak filaments in the honey-CNT film so that the memristor would return from the on-state back to the off-state within 2 min. Contrarily, the LTM "X" stimuli consist of a train of 30 voltage pulses (1.4 V, 10 ms) at a higher frequency of 50 Hz to form strong filaments in the honey-CNT film so that the memristor could remain in the on-state for 2 min or longer.

Figure 5(b) shows the voltage stimuli and output current response on each pixel before the memory test, at the last pulse of the applied stimuli, and 2 min thereafter. At the last pulse, the pixels that "E" and "X" overlap exhibit the highest current response, which indicates "strong" memory due to the combined stimuli. The non-overlapping pixels in "X" and "E" still show relatively high current, indicating that the array still "stored" the letters. After 2 min concluding the applied stimuli, only "X" pixels still showed a current response, although with lower amplitude, indicating that these memristors were still in the on-state and retained memory, while the non-overlapping "E" pixels all returned back to the off-state, i.e., "lost" memory. Such test results testify that STM and LTM can be manipulated by changing the stimuli via frequency and pulse number, much like in biological synapses. Currently, we are investigating approaches to scale up honey-CNT memristors so more pixels can be used to demonstrate the memory characteristics. These approaches include reducing the electrode sizes to accommodate more devices in a unit area, testing different coating techniques to improve the honey-CNT film uniformity, applying various mixing methods to disperse CNTs more uniformly in the honey

STDP is a type of biological long-term learning that standardly follows a Hebbian model. <sup>36,37</sup> In this model, the precise relative timing of action potentials (spikes) on a presynaptic neuron and a postsynaptic neuron directly affects the STDP. The magnitude of synaptic weight increases or decreases based on the relative timing between presynaptic and postsynaptic spikes. This leads to the overall strengthening or weakening of synaptic plasticity, i.e., potentiation or depression. Figure 6(a) depicts the analogy of a honey-CNT memristor to the biological synapse, and the application of the voltage pulses on the memristor to emulate STDP. Let  $\Delta \tau$  be the time interval between the postsynaptic spike and presynaptic spike, i.e.,  $\Delta \tau = t_{post} - t_{pre}$ . When the presynaptic spike is followed by the postsynaptic spike, i.e.,  $\Delta \tau > 0$ , it is expected that the synaptic plasticity increases, which leads to synaptic potentiation. When the postsynaptic spike is followed by the presynaptic spike, i.e.,  $\Delta \tau < 0$ , the synaptic plasticity decreases, which causes synaptic depression.

To emulate these presynaptic and postsynaptic spikes to verify the STDP behavior in the honey-CNT memristor, two voltage pulses with amplitude and width of 0.4 V and 20 ms but different time intervals  $\Delta \tau$  between 20 and 1000 ms were applied on the top electrode (pre-synapse) and the bottom electrode (post-synapse), respectively. The synaptic weight, or the change in EPSC before and after synaptic spikes, was mimicked using the output current (conductance) of the memristor before and after voltage pulses were applied, as

$$\Delta w = \frac{(I_{after} - I_{before})}{I_{before}} \times 100\% = \frac{(G_{after} - G_{before})}{G_{before}} \times 100\%, \quad (2)$$

where I is the current response, G is the conductance of the memristor, and subscripts "before" and "after" correspond to before and after voltage pulses applied on the device, respectively. Figure 6(b) shows the synaptic weight  $\Delta w$  as a function of time interval  $\Delta \tau$ , with a clear demonstration of potentiation and depression behaviors, which are dependent on the relative timing of the voltage pulses. This agrees with the STDP behaviors of biological synapses, which follow the symmetric

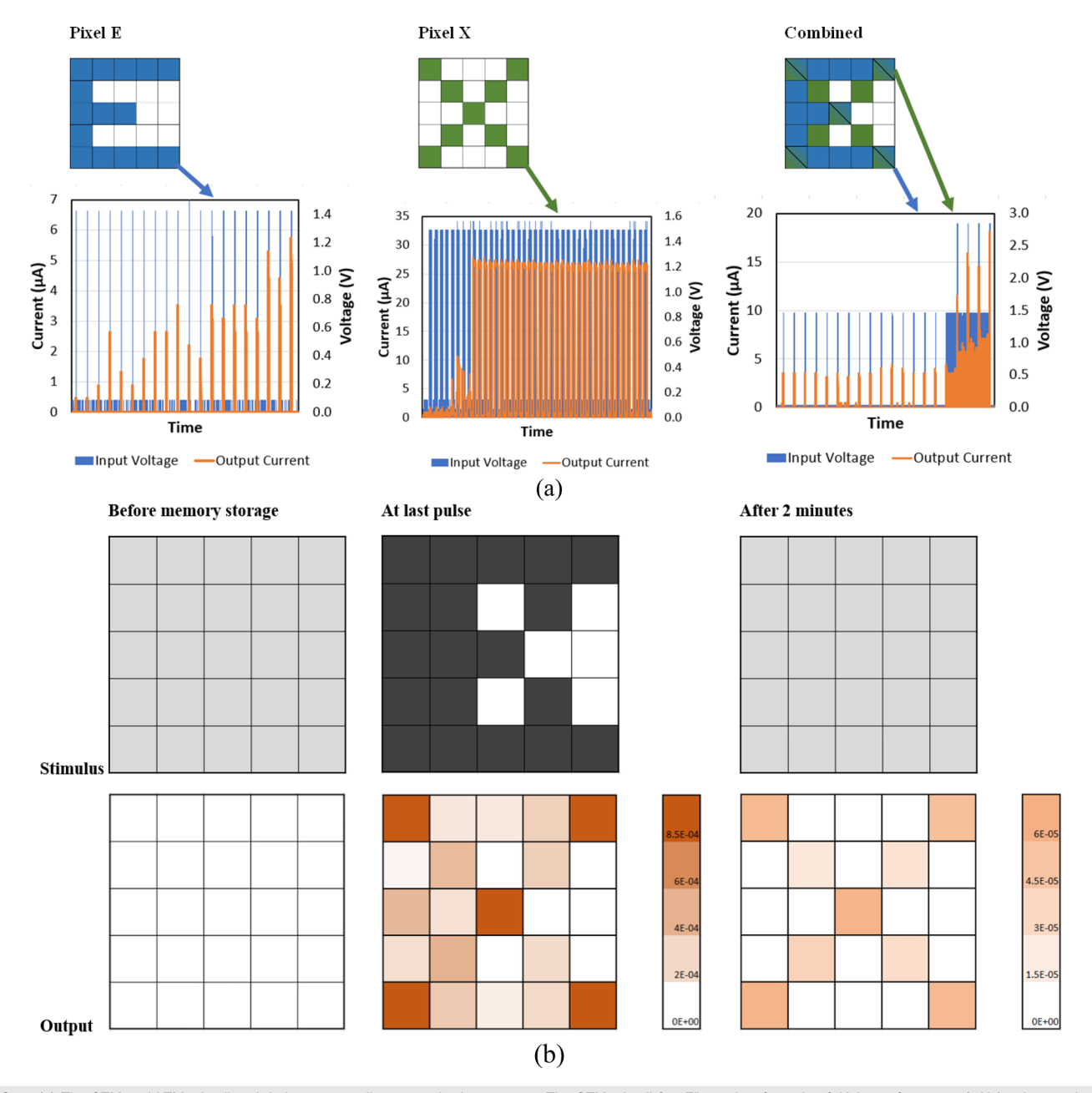


FIG. 5. (a) The STM and LTM stimuli and their corresponding memorization patterns. The STM stimuli for "E" consist of a train of 10 lower frequency (5 Hz) voltage pulses, while the LTM stimuli for "X" consist of a train of 30 higher frequency (50 Hz) voltage pulses with the same amplitude (1.4 V) and width (10 ms). (b) The applied stimuli and corresponding output current response of each pixel device before memory storage, at the last pulse, and 2 min after that stimuli were completed.

Hebbian learning rule<sup>36</sup> and can be modeled by an exponential decay function,

$$\Delta \tau > 0, \ w = A_{+} \exp\left(\frac{-\Delta \tau}{\tau^{+}}\right) \quad \Delta \tau < 0, \ w = A_{-} \exp\left(\frac{-\Delta \tau}{\tau^{-}}\right), \quad (3)$$

where  $A_+$  and  $A_-$  are the amplitude of the synaptic weight,  $\tau^+$  and  $\tau^-$  are the decay constants, and  $\Delta \tau$  is the relative timing.<sup>37</sup> The fitted lines

following Eq. (3) were also plotted in Fig. 6(b) and agreed well with the measurement data when  $A_+ = 429.3$ ,  $A_- = 470.7$ ,  $\tau^+ = 140$ , and  $\tau^- = 130$ .

It needs to be pointed out in Fig. 6(b) that when the honey-CNT memristor was tested with the relative timing in the range of 20–100 ms, which is observed in biological synapses, <sup>36</sup> a higher synaptic weight was achieved using voltage pulses with lower amplitude compared to other reported artificial synaptic devices made from

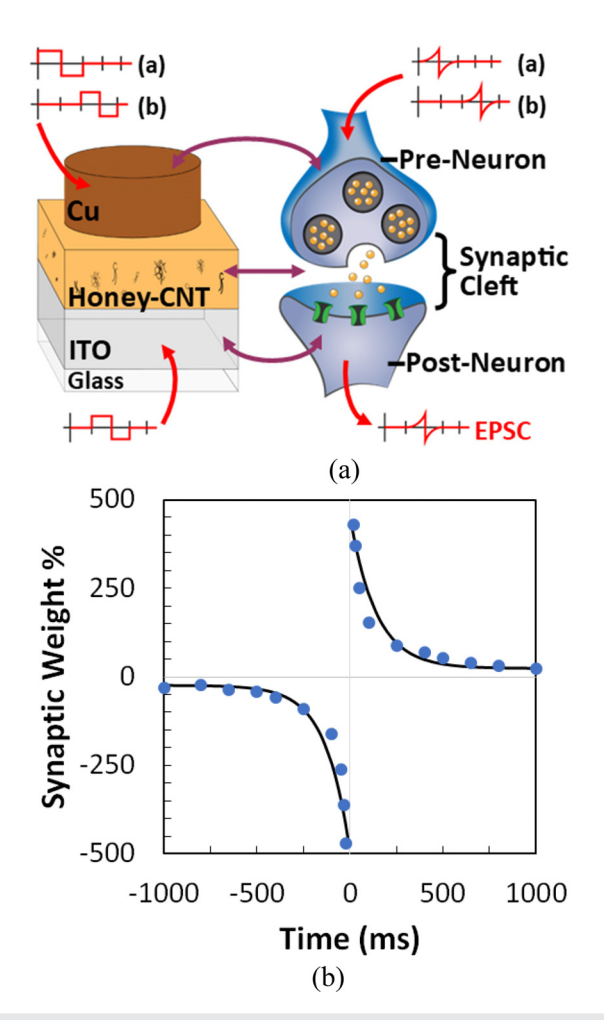


**FIG. 6.** STDP learning of honey-CNT memristor: (a) schematic analogy of the honey-CNT memristor to a biological synapse with voltage pulses applied on the electrodes to mimic presynaptic spikes in STDP and (b) the synaptic weight vs the relative timing from measurements (dots) and modeled by Hebbian-fitted curve.

natural biomaterials such as collagen and silk, <sup>8,38</sup> and even our previously reported pure honey. <sup>16</sup> Such higher gain is also attributed to the addition of CNTs in the honey film, which enhances the conductive filaments' growth under applied voltage pulses.

In summary, this work investigated honey-CNT memristors as artificial synaptic devices and their capabilities to emulate synaptic plasticity. A 206-level LTP and 206-level LTD for long-term memory was achieved, with the electrochemical mechanism explaining the formation and dissolution of conductive filaments during LTP and LTD, and compared to the biochemical mechanism that occurs in biological synapses. The STM and LTM behaviors via memorization of pixels onto a  $5\times 5$  array of devices attest to the uniformity and memorization repeatability of honey-CNT devices. PPF showed 800% gain, higher than those from other natural biomaterial-based memristors. STDP was emulated on a wider range of the stimuli pulse interval (20–2000 ms) and fitted to a typical STDP trend and also showed an improvement upon the gain in the 20 ms interval. These results

provide a useful insight into honey-CNT memristors as a promising building block for environment-friendly neuromorphic systems.

Feng Zhao acknowledges the support by the National Science Foundation under Grant Nos. 2104976 and 2247342. Zoe Templin acknowledges the support by the National Science Foundation Graduate Research Fellowship Program under Grant No. 2235552. The authors thank Andrew Templin for creating the schematic diagrams in the figures of this paper.

## AUTHOR DECLARATIONS Conflict of Interest

The authors have no conflicts to disclose.

### **Author Contributions**

Zoe Templin: Data curation (lead); Formal analysis (lead); Investigation (supporting); Methodology (lead); Validation (supporting); Writing – original draft (lead). Md Mehedi Hasan Tanim: Formal analysis (supporting); Investigation (supporting); Methodology (supporting); Validation (supporting). Feng Zhao: Conceptualization (lead); Funding acquisition (lead); Investigation (lead); Project administration (lead); Resources (lead); Supervision (lead); Validation (lead); Writing – review & editing (lead).

### **DATA AVAILABILITY**

The data that support the findings of this study are available from the corresponding author upon reasonable request.

### REFERENCES

- <sup>1</sup>H. Amrouch, N. Du, A. Gebregiorgis, S. Hamdioui, and I. Polian, "Towards reliable in-memory computing: From emerging devices to post-von-Neumann architectures," in *IFIP/IEEE 29th International Conference on Very Large Scale Integration (VLSI-SoC)* (IEEE, 2021), pp. 1–6.
- <sup>2</sup>P. Kiddee, R. Naidu, and M. H. Wong, "Electronic waste management approaches: An overview," Waste Manage. 33(5), 1237–1250 (2013).
- <sup>3</sup>S. M. Abdelbasir, S. S. M. Hassan, A. H. Kamel, and R. S. El-Nasr, "Status of electronic waste recycling techniques: A review," Environ. Sci. Pollut. Res. 25(17), 16533–16547 (2018).
- <sup>4</sup>G. W. Burr, R. M. Shelby, A. Sebastian, S. Kim, S. Kim, S. Sidler, K. Virwani, M. Ishii, P. Narayanan, A. Fumarola, L. L. Sanches, I. Boybat, M. Le Gallo, K. Moon, J. Woo, H. Hwang, and Y. Leblebici, "Neuromorphic computing using non-volatile memory," Adv. Phys. X 2(1), 89–124 (2017).
- <sup>5</sup>C. D. Schuman, S. R. Kulkarni, M. Parsa, J. P. Mitchell, P. Date, and B. Kay, "Opportunities for neuromorphic computing algorithms and applications," Nat. Comput. Sci. 2(1), 10–19 (2022).
- <sup>6</sup>L. Wang, S. Wei, J. Xie, and D. Wen, "Bioartificial synapses for neuromorphic computing," ACS Sustainable Chem. Eng. 11(6), 2229–2237 (2023).
- <sup>7</sup>T. Hussain, H. Abbas, C. Youn, H. Lee, T. Boynazarov, B. Ku, Y. R. Jeon, H. Han, J. H. Lee, C. Choi, and T. Choi, "Cellulose nanocrystal based biomemristor as a green artificial synaptic device for neuromorphic computing applications," Adv. Mater. Technol. 7(2), 2100744 (2022).
- <sup>8</sup>N. Raeis-Hosseini, Y. Park, and J. S. Lee, "Flexible artificial synaptic devices based on collagen from fish protein with spike-timing-dependent plasticity," Adv. Funct. Mater. 28(31), 1800553 (2018).
- <sup>9</sup>Y. Park and J. S. Lee, "Artificial synapses with short- and long-term memory for spiking neural networks based on renewable materials," ACS Nano 11(9), 8962–8969 (2017).
- <sup>10</sup>J. Wang, S. Mao, S. Zhu, W. Hou, F. Yang, and B. Sun, "Biomemristors-based synaptic devices for artificial intelligence applications," Org. Electron. 106, 106540 (2022).

- <sup>11</sup>B. Sun, T. Guo, G. Zhou, S. Ranjan, Y. Jiao, L. Wei, Y. N. Zhou, and Y. A. Wu, "Synaptic devices based neuromorphic computing applications in artificial intelligence," Mater. Today Phys. 18, 100393 (2021).
- <sup>12</sup>B. Sun, G. Zhou, T. Guo, Y. N. Zhou, and Y. A. Wu, "Biomemristors as the next generation bioelectronics," Nano Energy 75, 104938 (2020).
- generation bioelectronics," Nano Energy 75, 104938 (2020).

  <sup>13</sup>M. M. H. Tanim, Z. Templin, and F. Zhao, "Natural organic materials based memristors and transistors for artificial synaptic devices in sustainable neuromorphic computing systems," Micromachines 14(2), 235 (2023).
- <sup>14</sup>B. Sueoka, K. Y. Cheong, and F. Zhao, "Study of synaptic properties of honey thin film for neuromorphic systems," Mater. Lett. 308, 131169 (2022).
- 15B. Sueoka, K. Y. Cheong, and F. Zhao, "Natural biomaterial honey-based resistive switching device for artificial synapse in neuromorphic systems," Appl. Phys. Lett. 120(8), 083301 (2022).
- <sup>16</sup>B. Sueoka and F. Zhao, "Memristive synaptic device based on a natural organic material—honey for spiking neural network in biodegradable neuromorphic systems," J. Phys. D: Appl. Phys. 55(22), 225105 (2022).
- <sup>17</sup>B. Sueoka, M. M. Hasan Tanim, L. Williams, Z. Xiao, Y. Z. Seah, K. Y. Cheong, and F. Zhao, "A synaptic memristor based on natural organic honey with neural facilitation," Org. Electron. 109, 106622 (2022).
- <sup>18</sup> A. A. Sivkov, Y. Xing, K. Y. Cheong, X. Zeng, and F. Zhao, "Investigation of honey thin film as a resistive switching material for nonvolatile memories," Mater. Lett. 271, 127796 (2020).
- <sup>19</sup>M. M. H. Tanim, B. Sueoka, Z. Xiao, K. Y. Cheong, and F. Zhao, "Study of carbon nanotube embedded honey as a resistive switching material," Nanotechnology 33(49), 495705 (2022).
- <sup>20</sup>M. M. H. Tanim, Z. Templin, K. Hood, J. Jiao, and F. Zhao, "A natural organic artificial synaptic device made from a honey and carbon nanotube admixture for neuromorphic computing," Adv. Mater. Technol. 8(14), 2202194 (2023).
- <sup>21</sup>F. Daneshvar, H. Chen, K. Noh, and H. J. Sue, "Critical challenges and advances in the carbon nanotube-metal interface for next-generation electronics," Nanoscale Adv. 3(4), 942–962 (2021).
- <sup>22</sup>M. B. Jakubinek, B. Ashrafi, Y. Zhang, Y. Martinez-Rubi, C. T. Kingston, A. Johnston, and B. Simard, "Single-walled carbon nanotube-epoxy composites for structural and conductive aerospace adhesives," Composites, Part B 69, 87–93 (2015).
- <sup>23</sup>N. F. Zorn, F. Scuratti, F. J. Berger, A. Perinot, D. Heimfarth, M. Caironi, and J. Zaumseil, "Probing mobile charge carriers in semiconducting carbon nanotube

- networks by charge modulation spectroscopy," ACS Nano 14(2), 2412-2423 (2020)
- <sup>24</sup>A. Citri and R. C. Malenka, "Synaptic plasticity: Multiple forms, functions, and mechanisms," Neuropsychopharmacology 33(1), 18–41 (2008).
- <sup>25</sup>M. B. Kennedy, "Synaptic signaling in learning and memory," Cold Spring Harbor Perspect. Biol. 8(2), a016824 (2016).
- 26R. Lamprecht and J. LeDoux, "Structural plasticity and memory," Nat. Rev. Neurosci. 5(1), 45–54 (2004).
- <sup>27</sup>L. A. Santschi and P. K. Stanton, "A paired-pulse facilitation analysis of long-term synaptic depression at excitatory synapses in rat hippocampal CA1 and CA3 regions," Brain Res. 962(1-2), 78-91 (2003).
- <sup>28</sup>C. M. Powell, "Gene targeting of presynaptic proteins in synaptic plasticity and memory: Across the great divide," Neurobiol. Learn. Mem. 85(1), 2–15 (2006).
- <sup>29</sup>G. Wu, P. Feng, X. Wan, L. Zhu, Y. Shi, and Q. Wan, "Artificial synaptic devices based on natural chicken albumen coupled electric-double-layer transistors," Sci. Rep. 6, 23578 (2016).
- <sup>30</sup>C. Shi, J. Lan, J. Wang, S. Zhang, Y. Lin, S. Zhu, A. E. Stegmann, R. Yu, X. Yan, and X. Y. Liu, "Flexible and insoluble artificial synapses based on chemical cross-linked wool keratin," Adv. Funct. Mater. 30(45), 2002882 (2020).
- <sup>31</sup>E. P. Huang and C. F. Stevens, "Estimating the distribution of synaptic reliabilities," J. Neurophysiol. 78(6), 2870–2880 (1997).
- <sup>32</sup>W. G. Regehr, "Short-term presynaptic plasticity," Cold Spring Harbor Perspect. Biol. 4(7), a005702 (2012).
- 33S. Satake, T. Inoue, and K. Imoto, "Paired-pulse facilitation of multivesicular release and intersynaptic spillover of glutamate at rat cerebellar granule cell-interneurone synapses," J. Physiol. 590(22), 5653–5675 (2012).
- <sup>34</sup>T. V. P. Bliss and S. F. Cooke, "Long-term potentiation and long-term depression: A clinical perspective," Clinics 66, 3–17 (2011).
- 35R. Brette, "Philosophy of the spike: Rate-based vs. spike-based theories of the brain," Front. Syst. Neurosci. 9, 151 (2015).
- <sup>36</sup>D. E. Feldman, "The spike timing dependence of plasticity," Neuron **75**(4), 556–571 (2012).
- <sup>37</sup>K. D. Miller, L. F. Abbott, and S. Song, "Competitive Hebbian learning through spike-timing-dependent synaptic plasticity," Nat. Neurosci. 3, 919–926 (2000).
- <sup>38</sup>C. Shi, J. Wang, M. L. Sushko, W. Qiu, X. Yan, and X. Y. Liu, "Silk flexible electronics: From *Bombyx mori* silk Ag nanoclusters hybrid materials to mesoscopic memristors and synaptic emulators," Adv. Funct. Mater. 29(42), 1904777 (2019).